

LASER INTERFEROMETER GRAVITATIONAL WAVE OBSERVATORY
- LIGO -

CALIFORNIA INSTITUTE OF TECHNOLOGY
MASSACHUSETTS INSTITUTE OF TECHNOLOGY

Technical Note | LIGO-T952014-00 - R | 12/20/99

**Spatial Uniformity of Silicon
Photodiodes at Radio Frequencies**

Brian Lantz, David Shoemaker, Jamie Kerman

Distribution of this draft:

For submission to Applied Optics

California Institute of Technology
LIGO Project - MS 51-33
Pasadena CA 91125
Phone (818) 395-2129
Fax (818) 304-9834
E-mail: info@ligo.caltech.edu

Massachusetts Institute of Technology
LIGO Project - MS 20B-145
Cambridge, MA 01239
Phone (617) 253-4824
Fax (617) 253-7014
E-mail: info@ligo.mit.edu

1 ABSTRACT

The spatial uniformity of the sensitivity of EG&G DT110 silicon photodiodes to radio-frequency amplitude-modulated laser light was characterized. By raster-scanning the diodes under a beam much smaller than the diode, and recording the resulting signal variations from the detector, maps of the diode sensitivity were created. The fractional RMS fluctuation of the sensitivity was $6 \pm 1 \times 10^{-4}$, with a parabolic variation around the center of the diode as the principal component.

2 KEYWORDS

Photodiode; radio frequency; sensitivity; spatial uniformity

3 OVERVIEW

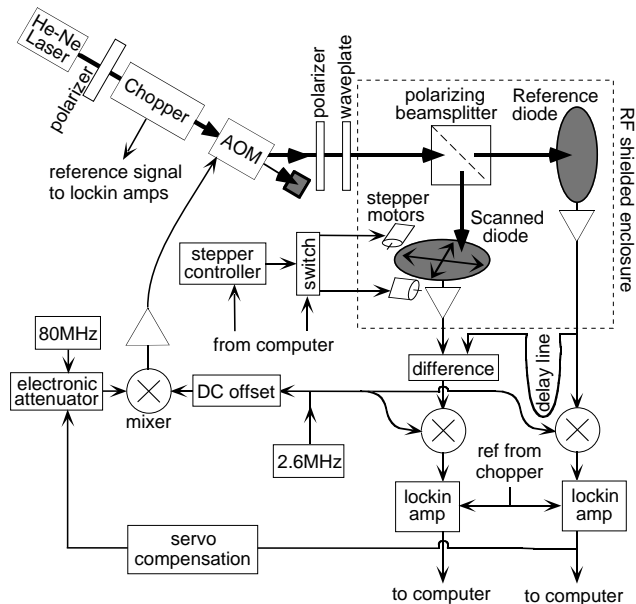
Silicon photodiodes are widely used to measure the intensity of light, due to their large dynamic range, fast response, high quantum efficiency, and ease of calibration. Knowledge of the spatial uniformity of the photodetector is important for many measurements, for example due to a need for high calibration precision¹, or due to changes in the beam position or intensity distribution on the photodiode leading to unintentional cross-coupling from spatial changes to measured photocurrent. Integrating spheres are often used to give independence of the measurement to the illumination pattern, but with a significant loss in overall optical efficiency. Measurements of the uniformity for steady-state signals have been made,^{1, 2, 3, 4, 5} but many applications use radio-frequency intensity modulation to carry the information on the light beam,^{6, 7, 8} and the spatial uniformity at these frequencies is the subject of these measurements.

Our specific application is the interferometric detection of gravitational radiation in the context of the LIGO Project⁹, where spatial non-uniformity of the photodiode can allow scattered light to become a source of noise in the detection system¹². The intensity at the antisymmetric port of a Michelson interferometer, held at the minimum of intensity, is measured with a photodiode. A TEM₀₀ gaussian laser beam is used to illuminate the interferometer, and a phase modulation system^{10, 11} is used to interrogate the interferometer to measure minute changes in the position of the interferometer's optical components. Light can scatter out of the main illuminating beam due to imperfections in the optical components, and through subsequent scattering (e.g., from a baffle in the vacuum system) can fall onto the photodetector, either by scattering directly onto the photodetector, or by recombining with the main beam at an optical surface. Light which recombines with the main beam has, in general, a negligible TEM₀₀ component, but can be described as a superposition of higher order TEM_{nm}, $n, m \neq 0$ modes. If the photodiode response is perfectly uniform and the photodiode is large (compared to the beam size), then the scattered light is

orthogonal to the principal TEM_{00} beam, and the overlap integral between the two will be zero due to the orthogonality of the different modes. Plane waves which scatter from e.g., a baffle onto the detector at an angle also have a spatially varying phase across the surface of the detector whose overlap integral with the main beam will approach zero if the detector is uniform. If, however, the photodiode response is spatially non-uniform, then this non-uniformity acts as a cross-coupling term between the scattered and principal light, and interference terms will lead to a sensitivity to these undesired paths.

Since length and angle detection in LIGO will be performed with light which is modulated at radio frequencies (RF), this experiment measured the response of the photodiode to light with RF amplitude modulation. These measurements were performed at 2.6 MHz, which was chosen for convenient modulation and demodulation.

Figure 1: The Experimental Setup



4 EXPERIMENTAL ARRANGEMENT

To map the sensitivity fluctuations of the diode, it was raster scanned under a laser beam which was intensity modulated at 2.6 MHz; changes in the output level of the scanned diode were interpreted as changes in the sensitivity. The intensity modulation was impressed on the light with an acousto-optic modulator, and the power in the 2.6 MHz band was kept constant with a feedback loop which monitored the light level with a stationary reference diode. To decrease the sensitivity to changes in the light level, and to better utilize the dynamic range of the electronics, the signal we examined was the difference of the scanned and reference diodes.

The experimental setup had several elements: the intensity-stabilized illumination source, the intensity modulator, the photodiodes and scanning system, the signal amplifiers and demodulators, and the data acquisition system. The layout of the experiment is shown in Figure 1, above.

The illumination source was a 1.3 mW He-Ne linearly polarized laser (PMS model STP 1M), enclosed in a thermally insulated box. The light was passed through a cleanup polarizer to insure that any variation of the polarization vector would result only in amplitude modulations at the beamsplitter. The light beam was mechanically chopped at 900 Hz to narrow the equivalent bandwidth of the measurement.

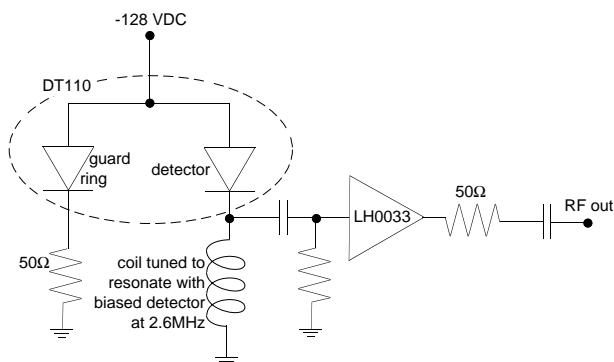
A servo loop using an Acousto-Optic Modulator (AOM) as actuator was used to keep the intensity of the beam delivered to the experiment constant to about 0.1% over the period of one scan. The light level is measured by the reference diode and the servo compensator drives an electronic attenuator for the 80MHz signal to the AOM. By varying the RF power driving the AOM, the intensity of the diffracted beam can be controlled. The loop had a single pole at 1Hz and an open loop DC gain of 80.

Using lenses (not shown in Figure 1), the beam size was optimized for the passage through the AOM and the other optics. The final focussing optics were chosen to give a beam spot size at the diode of $280\mu\text{m}$ ($1/e^2$ diameter). The grid spacing for the measurement points was $21\mu\text{m}$; this ratio insured that each data point was a good average of the portion of the diode being measured, so as to avoid aliasing of higher frequency spatial information.

To generate the intensity modulation at 2.6 MHz, the 80 MHz signal was mixed with a DC-biased 2.6 MHz signal, generating a signal at 80 MHz with a 2.6 MHz envelope, which was then applied to the AOM. This caused the diffracted beam from the AOM to be amplitude modulated at 2.6 MHz. The diffracted beam from the AOM passed through another clean-up polarizer, a waveplate (to adjust the linear polarization angle), and a polarizing beamsplitter. In this way, the balance of light between the diode being scanned and the reference diode could be adjusted.

All photodetectors used in the experiment were EG&G DT110 silicon photodiodes with the protective window removed (to eliminate effects of parasitic interferometers and inhomogeneity in the glass). The EG&G DT110 is a planar diffused, oxide passivated silicon photodiode with a circular active area of 1cm^2 (diameter of 1.13cm.) Each diode was mounted on a small box containing the amplifier circuit shown in Figure 2. An inductor forms a resonant circuit with the capacitance of the photodiode. This tuned circuit has a Q of 20, centered at 2.6 MHz. A voltage follower drives the 50Ω output line. The diode is reverse-biased with -128 VDC, which improves the diode response time, and has been shown to improve spatial uniformity at DC¹⁴.

Two detectors were used for a given measurement: the device under test (the scanned diode) was moved under the beam and mapped by the experiment, and the reference diode, which remained stationary with respect to the beam and was used to monitor the light level.

Figure 2: Diode detector and amplifier

The scanned diode and its preamplifier were mounted on a computer controlled x-y stage. The stage was moved in a square grid pattern with 44 data points along each side. After the diode was moved to a given location, the computer waited 0.1 seconds for the filters to settle, then recorded the differential scanned diode signal and the reference diode signal. The entire assembly of the final optics, the diodes and x-y stage were contained in a light-tight RF-shielded box.

The reference diode served two purposes. First, it was the detector for the servo system used to keep the intensity at the beamsplitter constant. Second, it acted as a reference level for the scanned diode, allowing the measurement of the scanned diode to be a differential, rather than absolute, measurement. Since the sensitivity variations were only about 0.1% of the overall sensitivity, a differential measurement scheme allowed better utilization of the dynamic range and resolution of the electronics and data acquisition system. In addition, this differential measurement technique made the experiment much more resistant to any residual light level fluctuations. Note that this scheme gives the system a second order sensitivity to phase shifts in the RF amplifiers.

The differential measurement was accomplished with a simple RF subtraction scheme which suppressed the large DC offset from the scanned diode; the recorded signal is the difference between the scanned diode and the reference diode, with the subtraction performed by a balanced RF transformer. The RF phases of the input signals are matched by varying coaxial cable lengths, and by tuning an adjustable “trombone” delay line. The amplitudes of the signals are balanced by adjusting the waveplate preceding the beamsplitter. At the beginning of each data run the beam was centered on the scanned diode and the apparatus adjusted so that the signal out of the differencing circuit was negligibly small.

The signal from the differencing circuit went to an amplifier/mixer box¹³ to mix the signal down from 2.6 MHz, and then to a lock-in amplifier, which mixed down the 900Hz chopping to the baseband. The output of the lock-in was low-pass filtered at 10 Hz before being recorded by the data acquisition computer (Concurrent model 6400 with an EF12M 12 bit data acquisition board).

In addition, the reference diode signal without differencing was also demodulated at 2.6 MHz and at 900 Hz as above. This signal was the reference for the intensity servo loop, and was recorded by the computer as a check on the system operation.

5 LIMITS OF THE MEASUREMENT SENSITIVITY

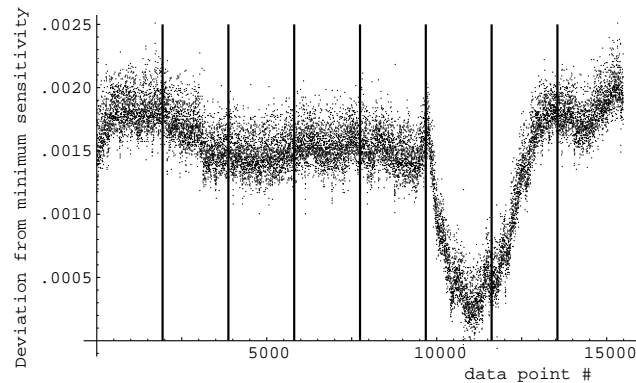
5.1. Instrumental Noise

To characterize the operational measurement noise, a series of “stationary scans” were made. A stationary scan was just like a data run, except the motor drives are disconnected, so that the scanned diode does not actually move. In this case, the signal should be perfectly constant, since one is continually measuring the response of the same point on the diode. Figure 3 shows a series of 8 sequential stationary data runs. Two kinds of noise can be seen in these data. There is some apparently stationary random measurement noise, so that repeated measurements should improve the signal-to-noise ratio. This noise has a fractional RMS level of 1.3×10^{-4} , and determines the sensitivity of our measurements. In addition, there are non-stationary changes in the signal, on the order of ten times the RMS noise, which occur once per 1-2 hours. These fluctuations must be recognized and excluded from the data, or they will improperly influence the results.

Each data run consisted of many scans of the diode. In order to identify and reject the infrequent non-stationary events, all the scans were averaged together, and the difference between each individual scan and the average scan was computed. The residuals of scans which were afflicted show large structural elements above the expected stationary noise, and these scans were excluded from further processing. Even if the scan looks quite rough (as is the case with the dusty photodiode, see Figure 8), one can say with confidence that the map accurately reflects the surface features of the diode, and is limited in sensitivity by the stationary noise.

The scanned diode was mounted on the amplifier box so that it was simple to rotate the diode by 180 degrees. As an additional test of the validity of the data, measurements were taken with the diode in both orientations, and then compared. The resulting measured structure rotates by 180 degrees, indicating that the structure is due to the photodiode non-uniformity.

LIGO-DRAFT

Figure 3: Stationary run. Eight sequential data runs

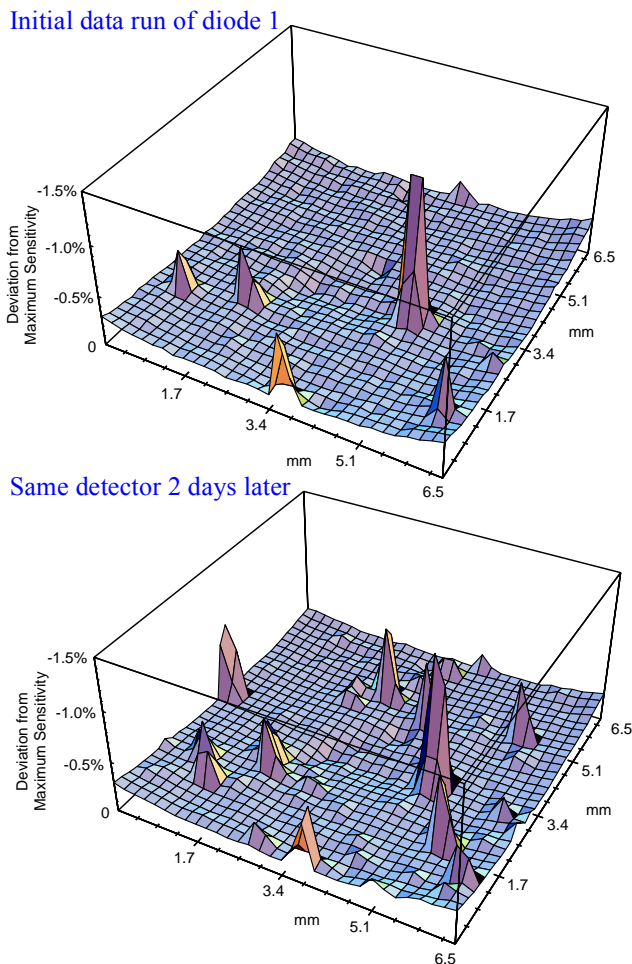
To determine the absolute sensitivity, the signal from the scanned diode was attenuated by a known amount (1.0 dB) and the output signal level recorded. Thus, 10.9% of absolute sensitivity was measured, allowing a scaling to be done for the scanned maps. The largest systematic error in our measurements is in the determination of the absolute magnitude of the average sensitivity, since the data were recorded as differential measurements. We estimate the absolute amplitude measurements to be no more accurate than $\pm 7\%$, which influences directly the uncertainty in the numerical value of the non-uniformity we deduce. We are interested in the spatial uniformity, not the average sensitivity, so errors in the absolute calibration are not critical to our application.

One anticipated limitation to the sensitivity of the measurement is the shot noise in the photocurrent. The fractional variation in a photocurrent I_{DC} in a one hertz bandwidth is given by $\delta i/I_{RF} = (\sqrt{2}\sqrt{2eI_{DC}})/I_{RF}$. For these measurements, the average photocurrent was 370 microamps, leading to a fractional variation of 5.8×10^{-8} in a one hertz bandwidth. The modulation/demodulation systems modify this by a small factor of order unity. This fundamental limitation is much smaller than the technical limitations discussed above, and can be neglected as a contribution.

5.2. Dust

It became apparent that dust was a problem from preliminary measurements. Figure 4 shows two data runs on diode 1, separated by an interval of two days, in which dust particles appear as narrow peaks. (These surface maps are inverted to better show the loss of sensitivity at particular pixels, and so a vertical increase indicates sensitivity decrease.) To alleviate this problem, a HEPA-filtered air source was added for the cooling of the metal box shielding the scanned and reference diodes. This greatly reduced the rate of dust accumulation.

Figure 4: Two data runs of Diode 1, about 2 days apart, showing dust accumulation. Note that the right picture contains the peaks from the earlier picture plus many additional ones.



6 RESULTS

Data were taken from one “mostly” clean diode (diode 1), two clean diodes (diode 2 and diode 3), and one “dusty” diode; each diode was scanned 15 to 30 times per run. All the analysis was done on a 32 by 32 grid of points taken from the center of the active area. The grid points were $211\mu\text{m}$ apart, so the measured square was 6.52 mm on a side, almost the largest square which could be inscribed on the diode. The square’s diagonal was 0.82 of the diode’s diameter.

The results from the clean diodes were very encouraging: the measured spatial variation in sensitivity was $6\pm 1 \times 10^{-4}$ of the average sensitivity (see Table 1), and the form and magnitude of the spatial response variations of diodes 1, 2, and 3 were essentially similar (see Figures 5-7).

By examining the three surface maps of the three clean diodes (Figures 5, 6, and 7, below), it is apparent that there is structure in the sensitivity of the diodes. The vertical scale on all the maps is given as the deviation from the normalized maximum sensitivity. Specks of dust cause dips in

the sensitivity, where the amplitude of these dips is not bounded by the -0.005 amplitude vertical scale limit. The diodes are most sensitive near the center and gradually lose sensitivity near the edges. One can fit a paraboloid to this response curve with a coefficient of $-10 \pm 2 \times 10^{-4} \left(\frac{\text{sensitivity}}{\text{mm}^2} \right)$ (see Table 1), and when the best fit paraboloid is removed from the data, the RMS of the residual is between 1.4×10^{-4} and 2.3×10^{-4} , essentially the noise limit of the measurement, implying that structure on the small spatial scale is still beyond the measurement precision of our apparatus. The curvature of the sensitivity is consistent with some DC measurements.^{4, 14} The RMS variation in sensitivity from the average sensitivity and the curvature of the best fit paraboloid is shown in Table 1, below, for each of the diodes. Some points on the diode were contaminated by dust which dramatically decreased the sensitivity. To calculate the dust-free RMS variation, these points were removed from the list of data, and the RMS of the shortened list was then calculated.

Table 1: RMS of Sensitivity Deviations for Diodes

| <i>Diode</i> | <i>RMS</i> | <i>RMS dust free</i> | <i>curvature</i> $\left(\frac{\text{sensitivity}}{\text{mm}^2} \right)$ |
|--------------|---------------------|----------------------|---|
| 1 | 10×10^{-4} | 5×10^{-4} | -9×10^{-5} |
| 2 | 8×10^{-4} | 7×10^{-4} | -12×10^{-5} |
| 3 | 6×10^{-4} | 6×10^{-4} | -8×10^{-5} |

For comparison, Figure 8 shows the map of a diode which was exposed to a dusty (class $\sim 10,000$) environment for several weeks. The dust accumulated on the surface completely dominates the map, with the measured structure quite repeatable. The RMS variation of this diode was 14×10^{-4} , while the RMS of the residuals (single scan - average scan) was only 3×10^{-4} . Dust can evidently easily dominate the spatial non-uniformity of the response of an exposed photodetector surface.

Power spectra of the two cleanest diodes were also computed. The Fourier transform of the sensitivity was calculated by averaging the power (amplitude squared) of the Fourier transform of each row and column of the 32 by 32 grid. The power spectra from diodes 2 and 3 are shown below in Figure 9. The best fit line shows the power falls off roughly proportional to the spatial frequency squared, i.e., $\left(\frac{\delta i(f)}{I_{\text{DC}}} \right)^2 \propto f^{(-2.2)}$ until the measurement falls into the noise. Note the apparent vertical scale difference; this may be consistent with the limited precision of our absolute calibration.

7 CONCLUSIONS

The spatial variation of the sensitivity of EG&G DT110 silicon photodiodes for radio-frequency (2.6 MHz) amplitude-modulated 634 nm laser light was measured and found to be quite small. The fractional RMS fluctuations of the sensitivity were $6 \pm 1 \times 10^{-4}$, with a parabolic variation around the center of the diode. For presently planned interferometers for gravitational-wave detection, this places the effect of recombination of scattered light at the photodetector well below other noise sources.

Figure 5: Surface Map of Diode 1

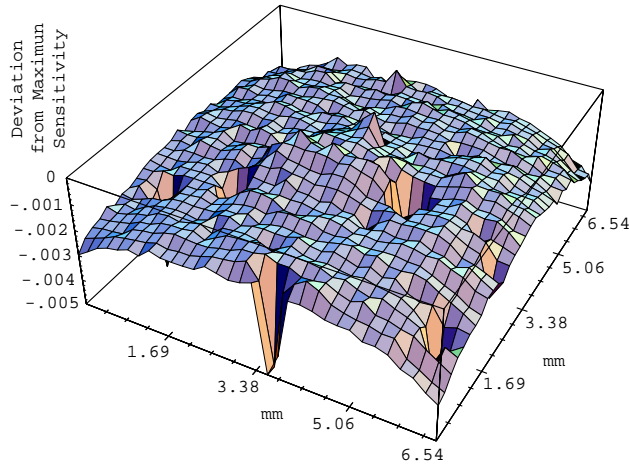
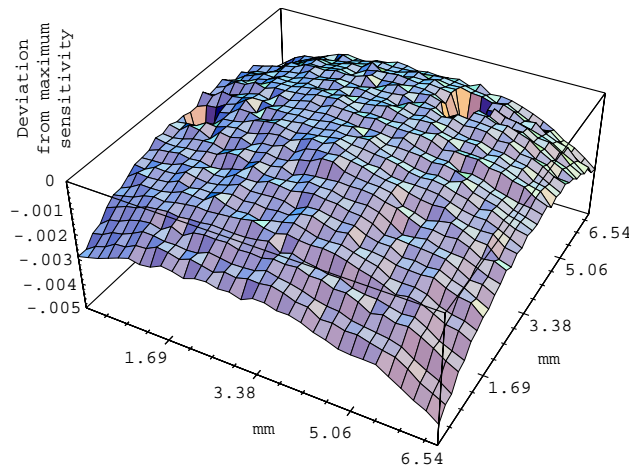


Figure 6: Surface Map of Diode 2



LIGO-DRAFT

Figure 7: Surface Map of Diode 3

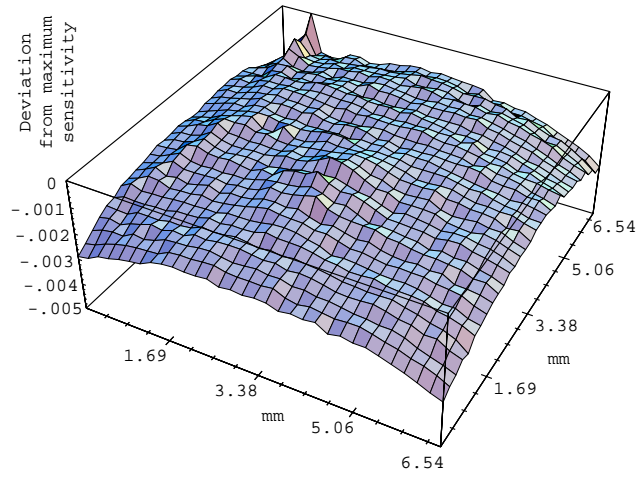
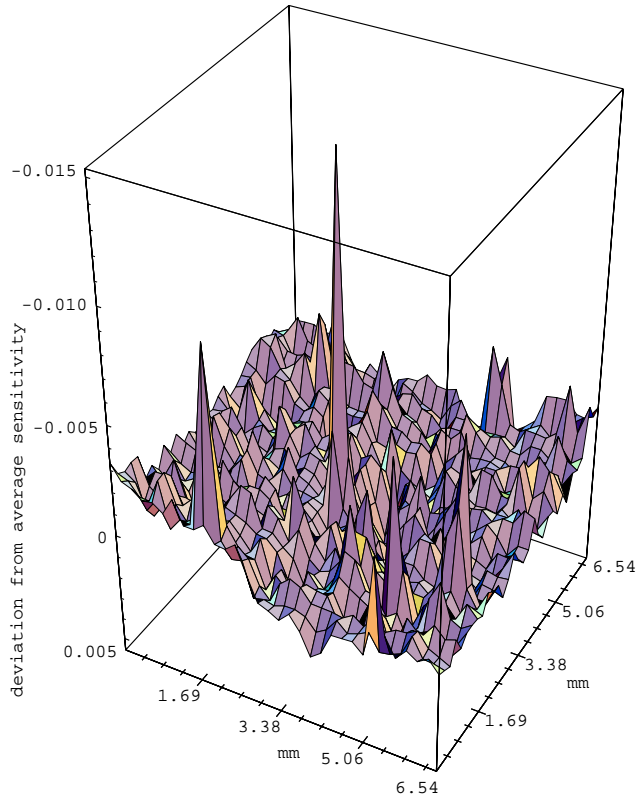
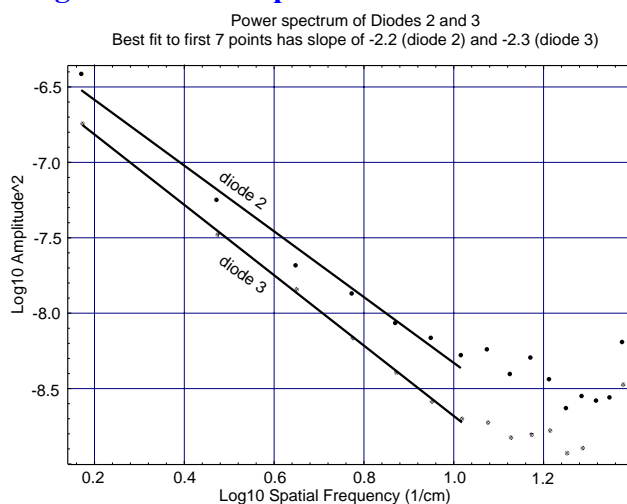


Figure 8: Surface Map of Dusty Diode



LIGO-DRAFT

Figure 9: Power Spectrum of Diode 2 and 3

8 REFERENCES

- 1: N. P. Fox, "Trap Detectors and their properties", *Metrologia*, 1991, **28**, 197-202.
- 2: Joaquin Campos, Antonion Corróns, and Alicia Pons, "Response uniformity of Silicon Photodiodes", *Appl. Opt.* **27**, 5154, (1988).
- 3: A. R. Schaefer, J. Geist, "Spatial Uniformity of Quantum Efficiency of a Silicon Photovoltaic Detector", *Appl. Opt.* **18**, 1933 (1979).
- 4: M. G. White, A. Bittar, "Uniformity of Quantum Efficiency of Single and Trap-configured Silicon Photodiodes", *Metrologia* 1993, **30**, 361-364.
- 5: A. Bittar, M. G. White, "High Resolution spatial uniformity of surface reflectance and response of silicon photodiodes", *SPIE Vol. 1712*, 14th Symposium of Photonic Measurements (1992), 121-131.
- 6: E. Morrison, B. J. Meers, D. I. Robertson, H. Ward, "Automatic Alignment of Optical Interferometers", *Appl. Opt.* **33**, 5041 (1994)
- 7: R. W. P. Drever, et. al., "Laser Phase and Frequency Stabilization Using an Optical Resonator", *Appl. Phys. B* **31**, 97-105 (1983)
- 8: Y. Hefetz, N. Mavalvala, D. Sigg, "Principles of Calculating Alignment Signals in Complex Resonant Optical Interferometers", *J. Opt. Soc. Am. B* **107**, 1597-1605 (1997)
- 9: A. Abramovici, et. al., "LIGO: the Laser Interferometer Gravitational-Wave Observatory", *Science* **256**, 325 (1992).
- 10: J. Giaime, "Studies of Laser Interferometer Design and a Vibration Isolation System for Interferometric Gravitational Wave Detectors", Massachusetts Institute of Technology Ph. D. Thesis (1995).
- 11: M. Regehr, F. Rabb, S. Whitcomb, "Demonstration of a power-recycled Michelson interferometer with Fabry-Perot arms by frontal modulation", *Optics Letters* **20** No. 13, (1995).

12: Kip Thorne, “Light Scattering and Proposed Baffle Configuration for the LIGO”, Internal LIGO Document, 11 January, 1989.

13: Paul Linsay, David Shoemaker, “Low-noise RF capacitance bridge transducer”, Review of Scientific Instruments, **53**, pg 1014 (1982).

14: A. R. Schaefer, E. F. Zalewski, and Jon Geist, “Silicon detector nonlinearity and related effects”, Appl. Opt. **22**, 1232 (1983).

15: B. Saleh and M. Teich, *Fundamentals of Photonics*, (John Wiley & Sons, Inc., New York, 1991).

LIGO-DRAFT